Mon. Not. R. astr. Soc. (1991) **252,** 428–441

EXOSAT observations of clusters of galaxies – II. X-ray to optical correlations

A. C. Edge★ and G. C. Stewart
X-ray Astronomy Group, Leicester University, Leicester LE1 7RH

Accepted 1991 May 30. Received 1991 May 30; in original form 1990 December 17

SUMMARY

The results obtained for clusters of galaxies using X-ray data from the European X-ray Observatory Satellite, *EXOSAT*, are compared with the optical, infrared and radio properties of the clusters taken from the literature. A number of strong correlations are found. The ratios of the intracluster medium (ICM) temperature and the cluster velocity dispersion, β, have a mean of less than one, in agreement with values obtained from the surface brightness distribution of the X-ray emission, thus resolving the 'Beta problem'. A particularly strong correlation exists between X-ray luminosity and spiral fraction indicating a direct link between the ICM and the structure of galaxies. The luminosity of the brightest cluster member and the X-ray properties of the cluster are found to be related, implying that its use as a standard candle should be corrected for the X-ray properties. The correlations between galaxy number density and X-ray properties imply mass-to-light ratios of 100–250 $h\,M_{\odot}/L_{\odot}$ in the cores of clusters and a ratio of gas mass to galactic mass of between one and two for all clusters. The implications of these results are reviewed.

1 INTRODUCTION

A number of samples of X-ray results for clusters have been compiled (Mitchell *et al.* 1979; Smith, Mushotzky & Serlemitsos 1979; McHardy 1978; Abramopoulos & Ku 1983; Jones & Forman 1984; Kowalski *et al.* 1984; Mushotzky 1984). These samples have shown that there are correlations between the X-ray and optical properties of clusters, e.g. galaxy number density and luminosity (Bahcall 1977a); spiral fraction and luminosity (Bahcall 1977b); velocity dispersion and luminosity (Quintana & Melnick 1982); optical luminosity and gas mass (Rothenflug & Arnaud 1985). These can be used to investigate the relationship between the galaxies in a cluster and the intra-cluster medium (ICM) in terms of their current interaction and evolution (Cavaliere & Fusco-Femiano 1976; De Young 1978). For example Cavaliere & Fusco-Femiano (1976) pointed out that the scaleheight for gas and galaxies in a cluster (referred to as β) can be determined in two ways. From imaging data where the surface brightness profile, $S(r)$, is of the form

$$S(r)=S_0\left[1+\left(\frac{r}{a}\right)^2\right]^{-3\beta+1/2}, \qquad (1)$$

where a is the core radius, β can be determined from the profile where $r \gg a$. And from optical and spectral data it is calculated as

$$\beta=\frac{\mu m\sigma^2}{kT}, \qquad (2)$$

where σ is the velocity dispersion, μm the mean particle mass and T the X-ray temperature. The two different values will be referred to as $\beta_{\rm imag}$ and $\beta_{\rm spec}$, respectively.

Previous results have given $\beta_{\rm imag}$ values in the range of 0.5–0.8 (Jones & Forman 1984) whereas $\beta_{\rm spec}$ lay between 0.8 and 3.0 (Mushotzky 1984). This discrepancy is known as the 'Beta problem' and has been seen as a major stumbling block for simple models of the ICM (Mushotzky 1984; Evrard 1990). To account for the difference, the ICM must be out of thermal equilibrium, perhaps through turbulent mixing of the ICM (Loewenstein & Fabian 1990) or the incomplete thermalization of infalling gas (Evrard 1990). Using the increased number of reliable velocity dispersions obtained and our improved data on ICM temperatures, we address this problem in greater detail.

Overall, the correlations between optical and X-ray properties confirm that both the galaxies and the ICM respond to the same potential, which is presumably dominated by 'Dark' Matter. From both optical and X-ray data it is possible to estimate the total contribution of 'luminous',

★Present address: Institute of Astronomy, Madingley Road, Cambridge CB3 0HA.

Table 1. The results from the X-ray spectral analysis.

Cluster	Temperature (keV)	Iron Abundance (relative to solar)	2-10 keV Flux ($erg\,cm^{-2}\,s^{-1}$)	Bolometric Correction	2-10 keV Luminosity ($erg\,s^{-1}$)	Bolometric Luminosity ($erg\,s^{-1}$)
A119	$5.1^{+1.0}_{-0.8}$	$0.28^{+0.26}_{-0.25}$	$3.02\pm0.09\times10^{-11}$	$2.19^{+0.10}_{-0.07}$	$2.57\pm0.08\times10^{44}$	$5.62\pm0.35\times10^{44}$
A133	$3.8^{+2.0}_{-0.9}$	< 1.1	$1.43\pm0.09\times10^{-11}$	$2.49^{+0.53}_{-0.35}$	$2.31\pm0.14\times10^{44}$	$5.75\pm1.11\times10^{44}$
A193	$4.2^{+1.6}_{-0.9}$	$0.57^{+0.64}_{-0.54}$	$1.34\pm0.09\times10^{-11}$	$2.34^{+0.30}_{-0.20}$	$1.37\pm0.10\times10^{44}$	$3.20\pm0.48\times10^{44}$
A262	2.4 ± 0.3	$1.31^{+0.94}_{-0.72}$	$2.34\pm0.09\times10^{-11}$	$3.58^{+0.58}_{-0.43}$	$2.63\pm0.12\times10^{43}$	$9.43\pm1.51\times10^{43}$
A376	$5.1^{+3.2}_{-1.9}$	< 0.70	$1.01\pm0.07\times10^{-11}$	$2.21^{+0.59}_{-0.10}$	$1.07\pm0.08\times10^{44}$	$2.35\pm0.42\times10^{44}$
AWM7	3.6 ± 0.2	$0.43^{+0.28}_{-0.25}$	$9.08\pm0.14\times10^{-11}$	$2.57^{+0.37}_{-0.25}$	$1.17\pm0.07\times10^{44}$	$3.00\pm0.45\times10^{44}$
A400	$2.1^{+1.3}_{-0.5}$	< 4.6	$0.79\pm0.08\times10^{-11}$	$4.27^{+1.79}_{-1.64}$	$1.86\pm0.17\times10^{43}$	$7.93\pm3.52\times10^{43}$
A3112	$4.1^{+2.3}_{-1.1}$	$0.81^{+0.96}_{-0.71}$	$1.94\pm0.15\times10^{-11}$	$2.39^{+0.28}_{-0.28}$	$4.82\pm0.37\times10^{44}$	$1.15\pm0.38\times10^{45}$
Perseus	5.5 ± 0.5	0.32 ± 0.03	$7.1\pm0.4\times10^{-10}$	$2.22^{+0.05}_{-0.04}$	$1.0\pm0.1\times10^{45}$	$2.3\pm0.1\times10^{45}$
0336+09	3.1 ± 0.3	$0.35^{+0.25}_{-0.23}$	$4.65\pm0.12\times10^{-11}$	$2.88^{+0.22}_{-0.18}$	$2.47\pm0.07\times10^{44}$	$7.12\pm0.64\times10^{44}$
A478	$6.8^{+1.1}_{-1.0}$	$0.27^{+0.14}_{-0.16}$	$6.54\pm0.18\times10^{-11}$	$2.11^{+0.04}_{-0.04}$	$2.28\pm0.08\times10^{45}$	$4.82\pm0.17\times10^{45}$
0422-09	$2.9^{+0.9}_{-0.6}$	< 1.6	$1.60\pm0.12\times10^{-11}$	$2.96^{+0.86}_{-0.48}$	$1.07\pm0.09\times10^{44}$	$3.15\pm0.73\times10^{44}$
A496	$4.7^{+1.0}_{-0.8}$	< 0.51	$5.37\pm0.23\times10^{-11}$	$2.27^{+0.19}_{-0.11}$	$2.40\pm0.42\times10^{44}$	$6.70\pm1.10\times10^{44}$
3C129	$5.6^{+0.7}_{-0.6}$	$0.20^{+0.11}_{-0.11}$	$9.00\pm0.28\times10^{-11}$	$2.27^{+0.06}_{-0.04}$	$1.89\pm0.14\times10^{44}$	$4.31\pm0.39\times10^{44}$
A576	$3.7^{+0.8}_{-0.6}$	$0.43^{+0.48}_{-0.41}$	$1.72\pm0.07\times10^{-11}$	$2.53^{+0.30}_{-0.23}$	$1.09\pm0.05\times10^{44}$	$2.76\pm0.36\times10^{44}$
0745-19	$8.5^{+1.9}_{-1.4}$	$0.29^{+0.14}_{-0.16}$	$5.71\pm0.15\times10^{-11}$	$2.17^{+0.07}_{-0.02}$	$2.72\pm0.70\times10^{45}$	$5.90\pm1.91\times10^{45}$
A754	$8.7^{+1.8}_{-1.6}$	< 0.37	$8.49\pm0.21\times10^{-11}$	$2.12^{+0.06}_{-0.02}$	$1.04\pm0.21\times10^{45}$	$2.21\pm0.75\times10^{45}$
Hydra-A	$3.9^{+1.0}_{-0.9}$	< 0.41	$2.44\pm0.24\times10^{-11}$	$2.46^{+0.51}_{-0.22}$	$2.93\pm0.29\times10^{44}$	$7.20\pm1.27\times10^{44}$
A1060	$3.3^{+0.4}_{-0.3}$	< 0.46	$4.35\pm0.12\times10^{-11}$	$2.70^{+0.23}_{-0.19}$	$2.45\pm0.08\times10^{43}$	$6.61\pm0.66\times10^{43}$
A1367	3.5 ± 0.5	< 0.29	$3.44\pm0.12\times10^{-11}$	$2.55^{+0.23}_{-0.18}$	$6.92\pm0.28\times10^{43}$	$1.76\pm0.19\times10^{44}$
Virgo	2.4 ± 0.3	0.4 ± 0.1	$3.3\pm0.2\times10^{-10}$	$3.43^{+0.55}_{-0.36}$	$1.1\pm0.1\times10^{43}$	$3.7\pm0.6\times10^{43}$
Coma	8.0 ± 0.3	0.21 ± 0.04	$3.2\pm0.2\times10^{-10}$	$2.13^{+0.01}_{-0.01}$	$7.4\pm0.4\times10^{44}$	$1.6\pm0.1\times10^{45}$
Centaurus	3.6 ± 0.4	$0.47^{+0.28}_{-0.26}$	$1.12\pm0.03\times10^{-10}$	$2.55^{+0.18}_{-0.14}$	$5.77\pm0.21\times10^{43}$	$1.47\pm0.13\times10^{44}$
A3562	$3.8^{+1.0}_{-0.8}$	$0.57^{+0.61}_{-0.56}$	$3.62\pm0.18\times10^{-11}$	$2.49^{+0.42}_{-0.23}$	$3.84\pm0.19\times10^{44}$	$9.55\pm1.34\times10^{44}$
A3571	$7.6^{+1.2}_{-0.9}$	$0.38^{+0.17}_{-0.18}$	$1.23\pm0.02\times10^{-10}$	$2.10^{+0.02}_{-0.02}$	$8.22\pm0.15\times10^{44}$	$1.73\pm0.50\times10^{45}$
A1795	$5.1^{+0.4}_{-0.5}$	$0.25^{+0.14}_{-0.12}$	$5.30\pm0.09\times10^{-11}$	$2.20^{+0.06}_{-0.04}$	$8.91\pm0.40\times10^{44}$	$1.96\pm0.12\times10^{45}$
A1837	$2.4^{+0.9}_{-0.8}$	< 11	$0.50\pm0.08\times10^{-11}$	$3.7^{+4.5}_{-1.4}$	$3.08\pm0.52\times10^{43}$	$1.12\pm0.42\times10^{44}$
A2052	$3.4^{+0.6}_{-0.5}$	$0.53^{+0.52}_{-0.43}$	$2.62\pm0.10\times10^{-11}$	$2.61^{+0.34}_{-0.26}$	$1.39\pm0.06\times10^{44}$	$3.63\pm0.26\times10^{44}$
A2142	$11.0^{+2.0}_{-1.7}$	< 0.36	$7.48\pm0.11\times10^{-11}$	$2.21^{+0.10}_{-0.07}$	$2.71\pm0.06\times10^{45}$	$5.99\pm0.32\times10^{45}$
A2147	$4.4^{+2.2}_{-1.1}$	< 1.1	$3.27\pm0.21\times10^{-11}$	$2.29^{+0.39}_{-0.18}$	$1.82\pm0.14\times10^{44}$	$4.16\pm0.62\times10^{44}$
A2199	4.7 ± 0.4	$0.21^{+0.13}_{-0.13}$	$7.12\pm0.10\times10^{-11}$	$2.25^{+0.06}_{-0.05}$	$2.97\pm0.43\times10^{44}$	$6.67\pm1.10\times10^{44}$
Tri. Aust.	$8.0^{+1.4}_{-1.3}$	$0.24^{+0.18}_{-0.16}$	$1.1\pm0.2\times10^{-10}$	$2.13^{+0.05}_{-0.03}$	$1.26\pm0.22\times10^{45}$	$2.69\pm0.48\times10^{45}$
Ophiuchus	$9.0^{+0.8}_{-0.7}$	$0.29^{+0.07}_{-0.08}$	$4.37\pm0.45\times10^{-10}$	$2.16^{+0.03}_{-0.02}$	$1.49\pm0.23\times10^{45}$	$3.22\pm0.52\times10^{45}$
S1101	$3.0^{+1.2}_{-0.7}$	< 1.5	$0.95\pm0.09\times10^{-11}$	$2.97^{+1.00}_{-0.59}$	$1.30\pm0.13\times10^{44}$	$3.85\pm1.07\times10^{44}$
A2589	$3.7^{+2.2}_{-1.1}$	< 2.0	$1.61\pm0.15\times10^{-11}$	$2.52^{+0.93}_{-0.39}$	$1.26\pm0.12\times10^{44}$	$3.17\pm0.75\times10^{44}$
A4059	3.5 ± 0.6	< 0.92	$1.88\pm0.08\times10^{-11}$	$2.58^{+0.33}_{-0.25}$	$1.89\pm0.14\times10^{44}$	$4.89\pm0.66\times10^{44}$

baryonic matter to the cluster and hence put limits on the 'Dark' Matter.

The principal properties of clusters derived from the X-ray data are the luminosity, temperature, iron abundance, core radius and the mass flow rate of any cooling flow. Here these are compared with the optical properties such as galaxy number density, velocity dispersion, fraction of spirals and absolute magnitude of the brightest cluster member.

Table 2. The optical data used in the analysis. The velocity dispersions are from the literature (see references). The velocity dispersion for A3112 is for the larger subcluster. The optical luminosities of the brightest galaxy are monochromatic at 5456 Å and within a metric radius of 38 kpc. The optical luminosities for A133 and A754 are from Valentijn & Bijleveld (1983), the rest are from Hoessel *et al.* (1980).

Cluster	Redshift	RS Type	BM Classes	D	R	Abell & Bahcall Number Densities		Velocity Dispersion (km s^{-1})		Calculated value of β_{spec}	Optical Luminosity of Central Galaxy (10^{10} $L_\odot$)
A119	0.0440(3)	C12	II-III	3	1	69	–	863^{+180}_{-130} (21)	[1]	$0.88^{+0.62}_{-0.32}$	13.5±2.7
A133	0.0604(3)	cD	I	4	0	47	–	–		–	12.0±2.5
A193	0.0482(3)	cDs	II	4	1	58	–	–		–	15.1±3.1
A262	0.0161(3)	C9	III	1	0	40	11	494^{+65}_{-50} (47)	[1]	$0.61^{+0.26}_{-0.17}$	–
A376	0.0489(5)	C7	I-II	3	0	36	–	–		–	–
AWM7	0.0172(7)	–	–	–	–	–	13	849^{+130}_{-90} (33)	[2]	$1.21^{+0.85}_{-0.45}$	–
A400	0.0232(3)	Ic	II-III	1	1	58	–	610^{+60}_{-50} (71)	[1]	$1.06^{+0.51}_{-0.50}$	8.1±1.7
A3112	0.0746(10)	–	I	3	2	116	–	820^{+160}_{-100} (23)	[3]	$1.00^{+0.96}_{-0.51}$	–
Perseus	0.0184(3)	L	II-III	0	2	88	32	1277^{+95}_{-80} (114)	[1]	$1.78^{+0.48}_{-0.34}$	–
0336+09	0.0349(3)	–	–	–	–	–	–	–		–	–
A478	0.0882(9)	cD	–	6	2	104	35	904^{+265}_{-140} (13)	[1]	$0.72^{+0.68}_{-0.28}$	–
0422-09	0.039(1)	–	–	–	–	–	–	–		–	–
A496	0.0320(4)	cD	I	3	1	50	14	705^{+100}_{-70} (39)	[1]	$0.64^{+0.36}_{-0.21}$	13.5±2.7
3C129	0.022(1)	–	–	–	–	–	–	–		–	–
A576	0.0381(5)	Ic	III	2	1	61	22	914^{+115}_{-85} (47)	[4]	$1.37^{+0.67}_{-0.44}$	–
0745-19	0.1028(3)	–	–	–	–	–	–	–		–	–
A754	0.0528(2)	cDs	I-II	3	2	92	29	747^{+85}_{-65} (59)	[1]	$0.39^{+0.19}_{-0.12}$	21.4±4.3
Hydra-A	0.0522(3)	–	I	–	–	–	–	–		–	–
A1060	0.0114(1)	C6	III	0	1	50	11	608^{+50}_{-40} (105)	[1]	$0.70^{+0.20}_{-0.15}$	–
A1367	0.0215(3)	F/I+I	II-III	1	2	117	18	822^{+70}_{-55} (93)	[1]	$1.15^{+0.40}_{-0.26}$	10.0±2.0
Virgo	0.0038(2)	–	III	–	–	–	10	573^{+35}_{-30} (159)	[5]	$0.82^{+0.24}_{-0.17}$	–
Coma	0.0232(3)	B	II	1	2	106	28	1010^{+55}_{-45} (234)	[1]	$0.77^{+0.11}_{-0.09}$	13.5±2.7
Centaurus	0.0109(2)	–	I-II	0	0	33	13	586^{+45}_{-35} (123)	[6]	$0.57^{+0.15}_{-0.13}$	–
A3562	0.0491(3)	–	I	2	2	129	–	–		–	–
A3571	0.0391(3)	–	I	2	2	126	–	1070^{+115}_{-90} (60)	[7]	$0.91^{+0.36}_{-0.25}$	–
A1795	0.0621(4)	cD	I	4	2	115	27	773^{+100}_{-75} (45)	[1]	$0.71^{+0.28}_{-0.17}$	14.5±2.9
A1837	0.0376(3)	cD	I-II	4	1	50	–	–		–	7.2±1.5
A2052	0.0348(3)	cD	I-II	3	0	41	–	576^{+85}_{-60} (61)	[8]	$0.58^{+0.31}_{-0.19}$	11.0±2.2
A2142	0.0899(11)	Bb	II	4	2	89	29	1241^{+330}_{-180} (15)	[9]	$0.84^{+0.74}_{-0.32}$	10.7±2.2
A2147	0.0356(10)	F/L+C	III	1	1	52	10	1148^{+190}_{-125} (30)	[10]	$1.81^{+1.47}_{-0.86}$	12.0±2.5
A2199	0.0309(3)	cD	I	1	2	88	18	794^{+80}_{-60} (71)	[11]	$0.80^{+0.24}_{-0.17}$	21.9±4.4
Tri. Aust.	0.051(1)	–	–	–	–	–	–	–		–	–
Ophiuchus	0.028(3)	–	–	–	–	–	–	–		–	–
S1101	0.0556(9)	–	III	3	0	28	–	–		–	–
A2589	0.0421(5)	cD	I	3	0	40	16	500^{+110}_{-70} (19)	[1]	$0.41^{+0.47}_{-0.22}$	–
A4059	0.0478(3)	–	I	2	1	66	–	845^{+280}_{-140} (11)	[12]	$1.24^{+1.38}_{-0.51}$	–

Notes: [1] Zabludoff, Huchra & Geller (1990); [2] Beers *et al.* (1984); [3] Materne & Hopp (1983); [4] Hintzen *et al.* (1982); [5] Binggeli, Tammann & Sandage (1987); [6] Lucey, Currie & Dickens (1986); [7] Quintana & de Souza (private communication); [8] Quintana *et al.* (1985); [9] Hintzen & Scot (1979); [10] Tarenghi *et al.* (1980); [11] Gregory & Thompson (1984); [12] Parker *et al.* (1986) and Green, Godwin & Peach (1988).

2 DATA

Details of the observations and the X-ray data used in this paper are presented and discussed in Edge & Stewart (1991) (Paper I). Table 1 summarizes the relevant spectral results. All X-ray luminosities are bolometric and corrected for galactic absorption. $H_0 = 50$ km s^{-1} Mpc^{-1}, $h = 1$ and $q_0 = 0.5$ are assumed throughout the analysis.

The compilation of a suitable, reliable optical dataset from the literature presented a number of problems. For example, Abell's visual estimates are the only systematic measurements of the galaxy number density of nearby clusters. These are unreliable on an individual basis (Lucey 1983). Values of the velocity dispersion (largely from Struble & Rood 1987), central galaxy number density (from Bahcall 1977a and 1981), spiral fraction (from Dressler 1980a and Bahcall 1977b) and the absolute magnitude of the brightest cluster member (from Hoessel, Gunn & Thuan 1980 and Valentijn & Bijleveld 1983) for at least 14 clusters in the sample in each case were available and are listed in Table 2.

It was shown in Paper I that the iron abundance is relatively constant for all clusters at ~ 0.3 of the solar value and seems to be unrelated to other cluster properties. Thus the iron abundance was not correlated with any of the optical properties. Also the mass flow rate is related to the X-ray luminosity so, to avoid indirect correlations with *global* cluster properties, the mass flow rate is only correlated with the luminosity of the Hα line.

3 THE OPTICAL CORRELATIONS

The most straightforward optical properties to correlate with the X-ray properties are the Bautz–Morgan and Rood–Sastry types which are related to the optical structure of the cluster. Table 3 gives the averages of temperature, bolometric luminosity and mass flow rate for the clusters with BM and RS types. There is a clear tendency for BM I and RS cD clusters (i.e. clusters with a single dominant galaxy) to have large cooling flows and a general trend for BM type III and RS types I and F to be cooler and less luminous. However, the sample is relatively small so it is not possible to draw any firm conclusions from optical structure alone.

Figs 1–11 show four optical properties plotted against X-ray luminosity and temperature. For the first four optical properties the least-squares fits for bolometric luminosity and temperature are plotted for both X-ray versus optical

Table 3. The average X-ray properties for different optical types (Bautz–Morgan and Rood–Sastry) with the rms scatter.

B-M Type	Number in Sample	Temperature (keV)	Bolometric Luminosity (erg s^{-1})	Mass Flow Rate ($M_\odot$ yr^{-1})
I	10	Ave=4.5±1.2	Ave=9.1±5.5 × 10^{44}	Ave=194±166
I-II	5	Ave=4.6±2.5	Ave=9.2±5.4×10^{44}	Ave=35±31
II	3	Ave=7.74±3.78	Ave=8.5±11.0 × 10^{44}	Ave=83±139
II-III	4	Ave=4.1±1.6	Ave=7.8±10.4 × 10^{44}	Ave=69±117
III	6	Ave=3.2±0.8	Ave=1.5±1.5 × 10^{44}	Ave=60±95
R-S Type	–	–	–	–
cD	18	Ave=5.1±2.1	Ave=1.6±1.4 × 10^{45}	Ave=209±208
B	2	Ave=9.5±1.5	Ave=3.8±2.2 × 10^{45}	Ave=125±125
C	4	Ave=3.9±1.3	Ave=2.4±2.2 × 10^{44}	Ave=20±7
I	2	Ave=2.9±0.7	Ave=1.8±1.4 × 10^{44}	Ave=25±17
F	2	Ave=4.0±0.4	Ave=3.0±1.7 × 10^{44}	Ave=30±30

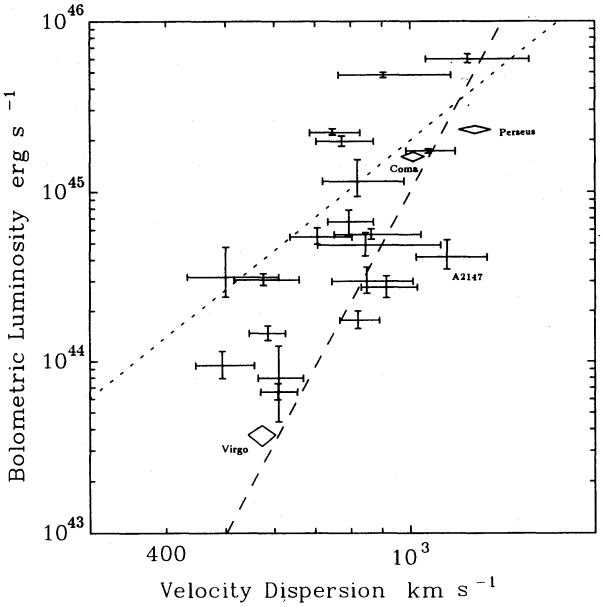

Figure 1. Bolometric X-ray luminosity against velocity dispersion. Perseus, Coma and Virgo are marked with diamonds.

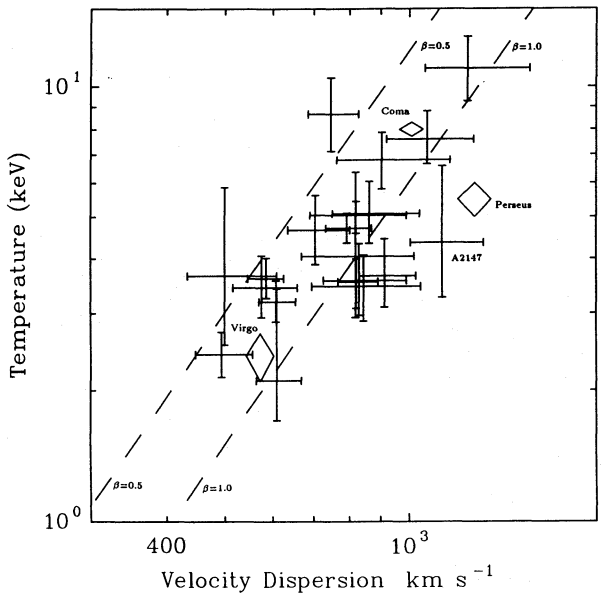

Figure 2. Temperature against velocity dispersion. Symbols are as in Fig. 1. Lines of $\beta = 0.5$ and 1.0 are plotted.

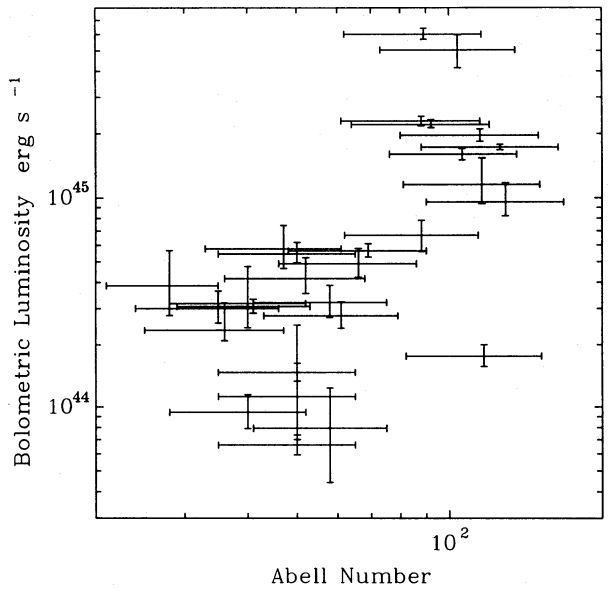

Figure 3. Bolometric X-ray luminosity against Abell galaxy number.

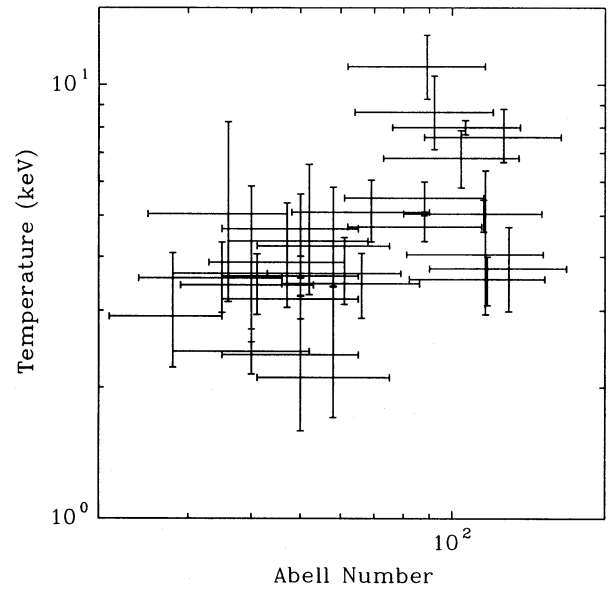

Figure 4. Temperature against Abell galaxy number.

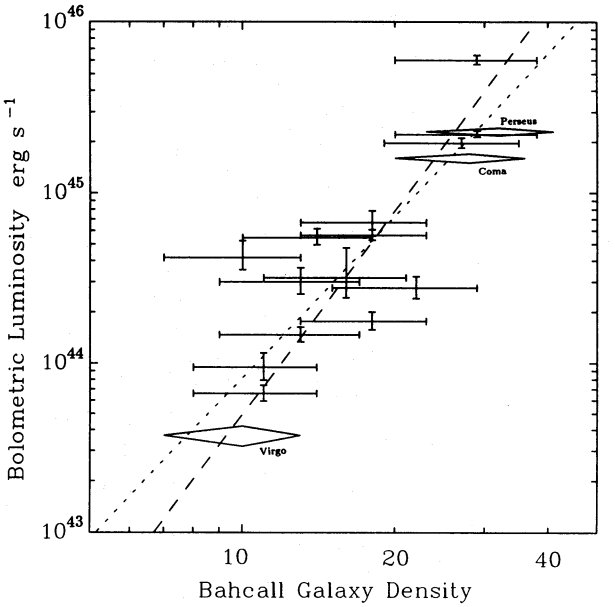

Figure 5. Bolometric X-ray luminosity against Bahcall galaxy number density.

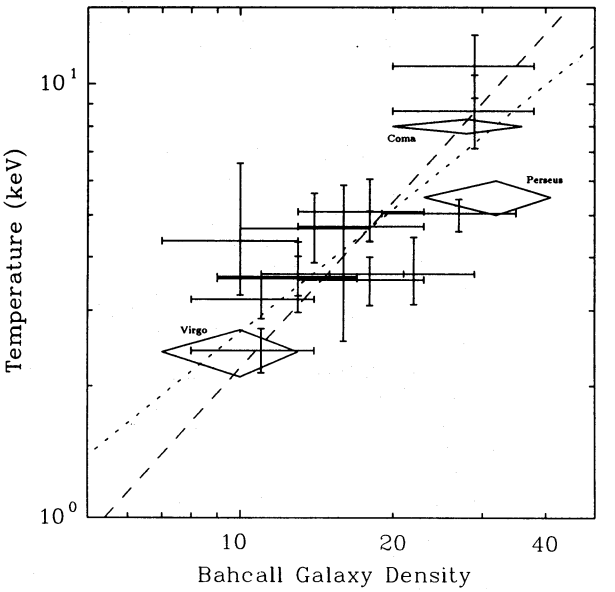

Figure 6. Temperature against Bahcall galaxy number density.

data and vice versa (apart from T versus σ). All the correlations are significant at the 99 per cent level and have been examined for secondary correlations through redshift and these are excluded at the 95 per cent confidence level. Because of the strong interrelations between all the X-ray and optical properties, it is difficult to determine which of the correlations is primary. This is particularly difficult in the case of the luminosity and temperature which are well correlated but with a significant scatter (Paper I). Each property is discussed below.

3.1 Velocity dispersion

The velocity dispersion is the optical property which is believed to be most closely related to the mass of a cluster. A correlation between velocity dispersion and X-ray luminosity has been well established (Quintana & Melnick 1982), but the correlation with temperature was less certain (Mushotzky 1988). Figs 1 and 2 show that there exist strong correlations with both X-ray luminosity and gas temperature. The least-squares fits for the 23 clusters in the sample with velocity dispersion are

$$L_{\rm bol} = 10^{36.60\pm0.55}\,\sigma^{2.90\pm0.19} \qquad r = 0.594 \qquad \text{or}$$

$$\sigma = 10^{-3.75\pm0.17}\,L_{\rm bol}^{0.15\pm0.05} \qquad r = 0.759$$

$$T = 10^{-3.22\pm0.77}\,\sigma^{1.35\pm0.27} \qquad r = 0.807 \qquad \text{or}$$

$$\sigma = 10^{2.60\pm0.08}\,T^{0.46\pm0.12} \qquad r = 0.743,$$

where $L_{\rm bol}$ is in erg s^{-1}, T in keV and σ in km s^{-1}.

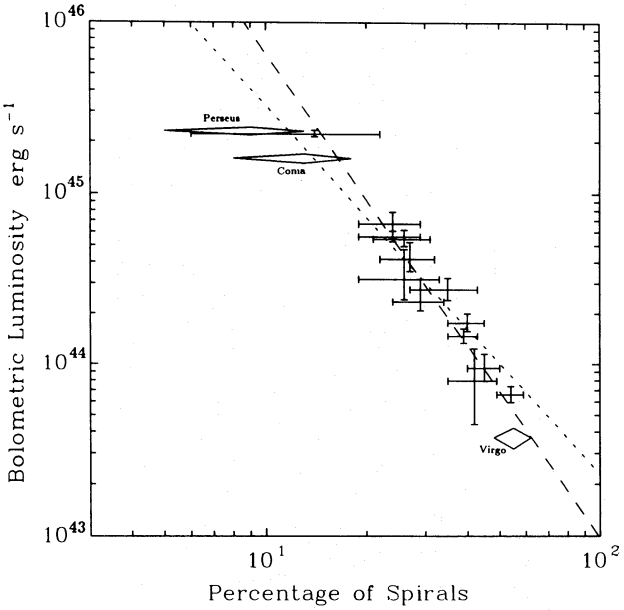

Figure 7. Bolometric X-ray luminosity against percentage of spiral galaxies.

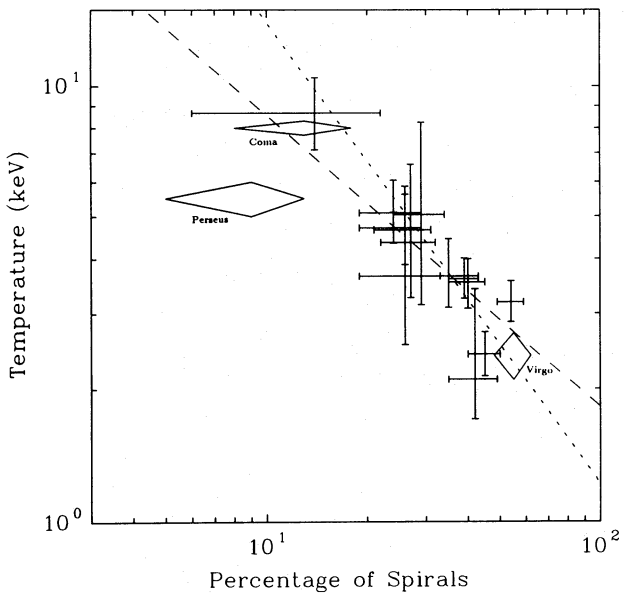

Figure 8. Temperature against percentage of spiral galaxies.

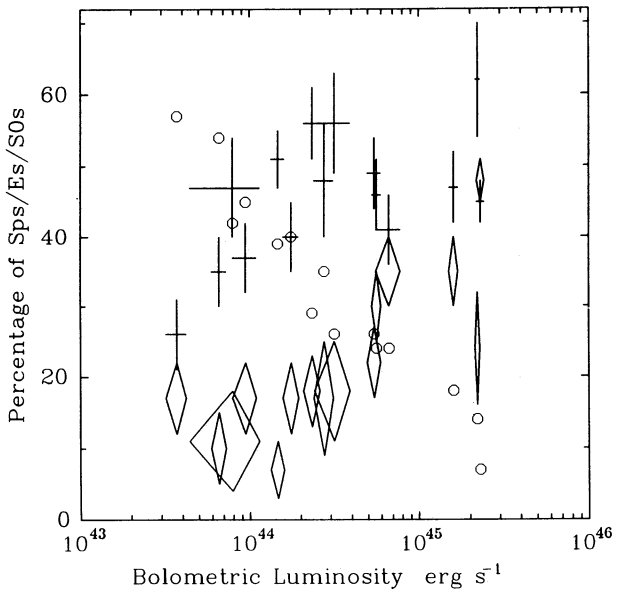

Figure 9. Bolometric X-ray luminosity against percentage of spiral, lenticular and elliptical galaxies. The spiral, lenticular and elliptical percentages are marked as circles, crosses and diamonds, respectively.

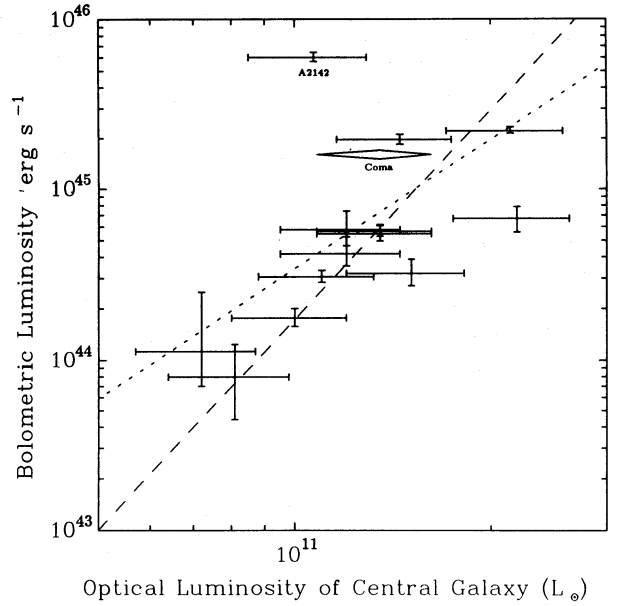

Figure 10. Bolometric X-ray luminosity against optical luminosity of the brightest cluster member.

Considerable scatter to high velocity dispersion exists with both luminosity and temperature. As the velocity dispersion and temperature are both believed to be closely related to the mass of the cluster (from virial and hydrostatic assumptions), then the correlation between the two should be the primary one. However, the scatter in the velocity dispersions due to subclustering and measurement difficulties (Fitchett & Webster 1987) makes it very difficult to disentangle the two. The problems related to the optical determination of velocity dispersion and the implications of the temperature–velocity dispersion correlation are discussed in more detail in Section 4.1.

3.2 Galaxy number density

On the assumptions of a constant mass-to-light ratio and similar form for the galaxy luminosity function for all clusters, then the galaxy number density (usually quoted as the number of galaxies within a certain magnitude range and radius) should be closely related to the cluster mass (Colless 1989). The largest available dataset of galaxy densities/counts are those of Abell (1958) and Abell, Corwin & Olowin (1989) which form the basis of the Abell classification scheme. Figs 3 and 4 show these galaxy counts within 3

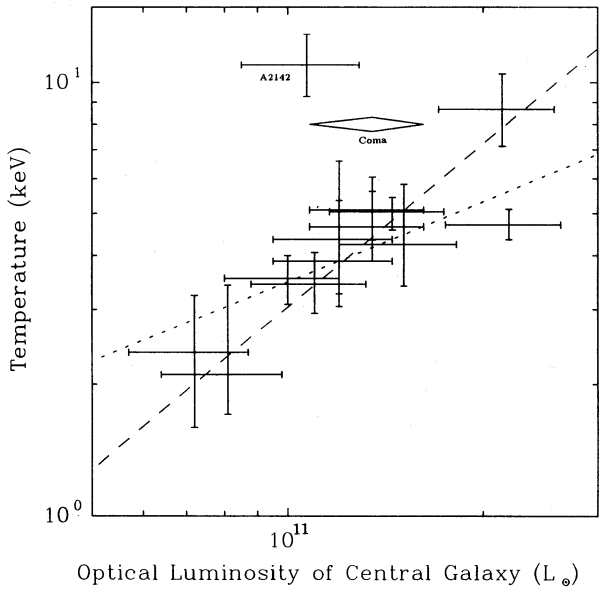

Figure 11. Temperature against optical luminosity of the brightest cluster member.

Mpc compared with luminosity and temperature. There is a general trend for a higher Abell Number with increasing X-ray luminosity and temperature but the scatter and the error in galaxy number are relatively large (30 per cent).

Clearly a more reliable measure of the galaxy number density is required. The best measure in the literature is provided by Bahcall (1977a, 1981) who counted the number of galaxies in a magnitude range within 0.5 Mpc, thus reducing the chances of confusion with other nearby clusters and foreground or background groups. Figs 5 and 6 show correlations between Bahcall galaxy densities and luminosity and temperature. The least-squares fits for the 18 clusters in the sample with Bahcall galaxy number densities give

$$L_{\rm bol} = 10^{40.75\pm0.20} N_{\rm B}^{3.16\pm0.15} \qquad r = 0.903 \qquad \text{or}$$

$$N_{\rm B} = 10^{-9.53\pm0.65} L_{\rm bol}^{0.25\pm0.14} \qquad r = 0.859$$

$$T = 10^{-0.52\pm0.24} N_{\rm B}^{0.95\pm0.18} \qquad r = 0.876 \qquad \text{or}$$

$$N_{\rm B} = 10^{0.73\pm0.31} T^{0.78\pm0.47} \qquad r = 0.793,$$

where $L_{\rm bol}$ is in erg s^{-1}, T in keV and $N_{\rm B}$ in number of galaxies.

The correlations appear to be stronger than those with Abell number, although fewer clusters have Bahcall numbers. The approximately linear relationship between temperature and galaxy density indicates that the fraction of the total cluster mass in the form of galaxies is roughly constant from groups of galaxies to very rich clusters and is consistent with previous work (Mushotzky 1984). By combining this with the fractions of total cluster mass in ICM gas, the relative ratios of gas and galaxies may be determined (see Section 4.3).

3.3 Spiral fraction

The relative populations of galactic types in clusters have been shown to be closely related to their local environment (Melnick & Sargent 1977; Dressler 1980b; Giovanelli & Haynes 1985). Figs 7 and 8 show the fraction of spirals plotted against luminosity and temperature. The least squares fits for the 16 clusters in the sample with published spiral fractions give:

$$L_{\rm bol} = 10^{43.35\pm0.14} f_{\rm sp}^{-2.16\pm0.11} \qquad r = -0.957 \qquad \text{or}$$

$$f_{\rm sp} = 10^{15.06\pm0.50} L_{\rm bol}^{-0.35\pm0.12} \qquad r = -0.960$$

$$T = 10^{0.26\pm0.16} f_{\rm sp}^{-0.67\pm0.12} \qquad r = -0.900 \qquad \text{or}$$

$$f_{\rm sp} = 10^{0.08\pm0.21} T^{-0.94\pm0.38} \qquad r = -0.800,$$

where $L_{\rm bol}$ is in erg s^{-1}, T in keV and $f_{\rm sp}$ in fraction of spirals.

The very strong correlation with luminosity has been noted previously (Bahcall 1977b; McHardy 1978). The scatter in Fig 7 is remarkably small and indicates that the primary correlation is with the luminosity (i.e. ICM density and volume) rather than temperature (cluster potential). This, in turn, implies that the X-ray luminosity is a better measure of the 'mean' ICM pressure than the temperature, due mainly to the large variation in the gas mass fraction (see Paper I). Fig. 9 shows the fraction of spirals, lenticulars (S0s) and ellipticals (Es) against X-ray luminosity. The trend for increasing S0 and E populations with increasing X-ray luminosity is very similar to that seen in Dressler (1980b) for galaxy density. The greater scatter seen in the S0 and E populations may result from the difficulty in differentiating between them when the S0 is face on (van den Bergh 1990). This result has important implications for models of how galaxies interact with the ICM, which are discussed in Section 4.2.

3.4 Luminosity of brightest cluster member

A trend for the optical luminosity of the brightest galaxy in a cluster to increase with the X-ray luminosity has been noted by Schombert (1988). Figs 10 and 11 show strong correlations between the optical luminosity of the brightest galaxy member (BCM) and the X-ray luminosity and temperature, indicating that the galaxy responds to the underlying cluster. The least-squares fits for the 12 clusters in the sample with BCM luminosities give:

$$L_{\rm bol} = 10^{14.09\pm0.29} L_{\rm BCM}^{2.53\pm0.22} \qquad r = 0.870 \qquad \text{or}$$

$$L_{\rm BCM} = 10^{-1.13\pm0.78} L_{\rm bol}^{0.27\pm0.17} \qquad r = 0.822$$

$$T = 10^{-6.23\pm0.42} L_{\rm BCM}^{0.62\pm0.36} \qquad r = 0.724 \qquad \text{or}$$

$$L_{\rm BCM} = 10^{10.62\pm0.29} T^{0.80\pm0.45} \qquad r = 0.876,$$

where $L_{\rm bol}$ is in erg s^{-1}, T in keV and $L_{\rm BCM}$ in solar luminosities.

These correlations are consistent with the observation of alignment of cDs with their cluster noted by Rhee & Roos (1990) in that cluster and central galaxy are linked. However, they contradict the notion that these galaxies are in some way 'special' and unrelated to the parent cluster (Bhavsar 1989).

The only exceptions to the correlation are clusters that contain two bright galaxies, such as Coma and A2142. These clusters have brightest galaxies which have optical luminosities a factor of approximately two below those expected from the correlation with cD galaxies. The relationship would hold, however, for the sum of the two brightest galaxies. These clusters may be the result of the merger of two clusters of approximately the same mass in which the

two cD galaxies do not merge or merge slowly (Tremaine 1990). The frequency of such cluster–cluster mergers is consistent with the observed cluster evolution (Edge *et al.* 1990).

The relationship between the luminosity of brightest cluster members and the X-ray properties implies that BCMs cannot be used as standard candles, since they are not all of the same luminosity. However, in combination with X-ray data, it is possible to develop a much more accurate standard which significantly improves the Hubble Diagram (Edge 1991).

3.5 Optical line emission

A number of studies of the extended line emission surrounding central galaxies have been made (Cowie *et al.* 1983; Hu, Cowie & Wang 1985; Johnstone, Fabian & Nulsen 1987). The exact nature of the line emission is poorly understood (Cowie, Fabian & Nulsen 1980) but must be related to gas at 10^4–10^6 K which cools through emission of recombination and forbidden lines. Taking the estimated mass of cooling gas from the X-ray data, then the expected Hα luminosity is several hundred times lower than observed if each cooling proton recombines once.

Fig. 12 shows the relationship between the luminosity in the Hα and N II blend and the mass flow rate in cooling clusters. This should be a direct correlation, as clusters which are not cooling do not exhibit line emission (Johnstone, Fabian & Nulsen 1987). However, there are cases where there is evidence for cooling in the X-ray data but no detectable optical line emission (e.g. A2029). In addition, the dispersion in the relationship is large. Fig. 12 shows that clusters with $\dot{M}=100$–$200\ M_\odot\ \mathrm{yr}^{-1}$ have line luminosities which differ by factors of up to 100 (2×10^{40}–2×10^{42} erg s^{-1}). Clearly, although there is a link between line emission and the cooling flow, it is not straightforward.

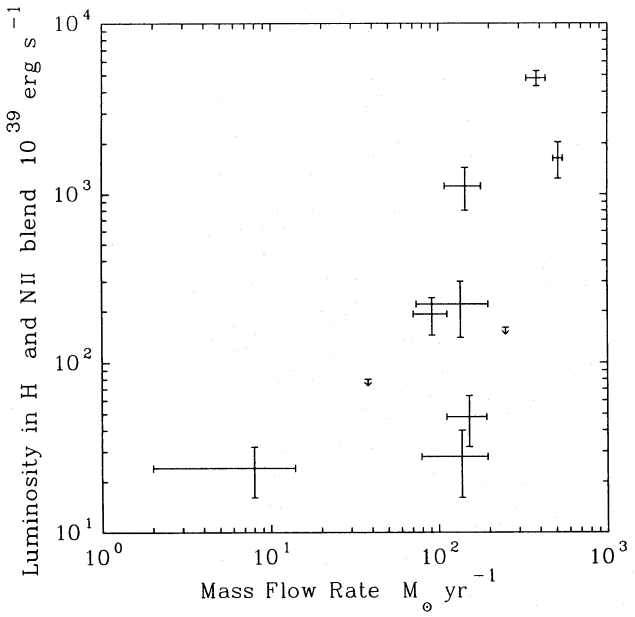

Figure 12. Luminosity of Hα line emission against total mass flow rate.

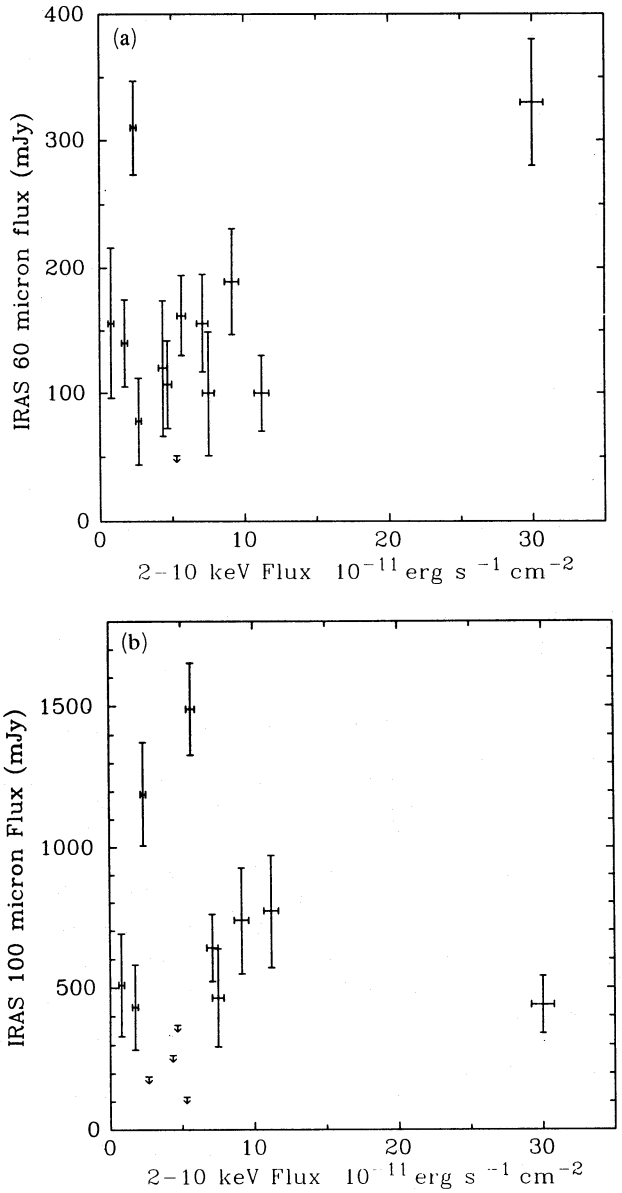

Figure 13. (a) and (b) *IRAS* 60- and 100-μm flux plotted against 2–10 keV X-ray flux.

3.6 Far-infrared emission

Recent work by Bregman, McNamara & O'Connell (1990) shows that the far-infrared luminosities of cD galaxies detected by *IRAS* are of the order of 10^{43-44} erg s^{-1}. The *IRAS* fluxes are close to the detection limit and are liable to confusion with foreground stars or AGN. Figs 13(a) and (b) show the *IRAS* 60- and 100-μm fluxes plotted against 2–10 keV flux for clusters common to the two samples with the addition of Virgo and Centaurus (from Leggett *et al.* 1987 and Jura *et al.* 1987). There is substantial scatter but with a general trend for brighter X-ray clusters to be brighter in the *IRAS* bands. Bregman *et al.* discuss the possibility of the *IRAS* sources being due to confusing stars and conclude that only two or three may be confused with stars. Fig. 14 shows an apparently correlation between X-ray and *IRAS* luminosities, but this is mainly an artefact of comparing the

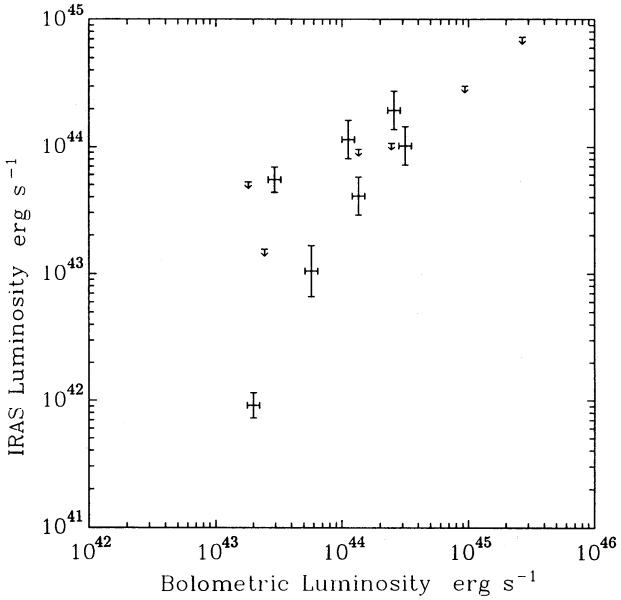

Figure 14. *IRAS* luminosity from Bregman *et al.* (1990) against bolometric X-ray luminosity.

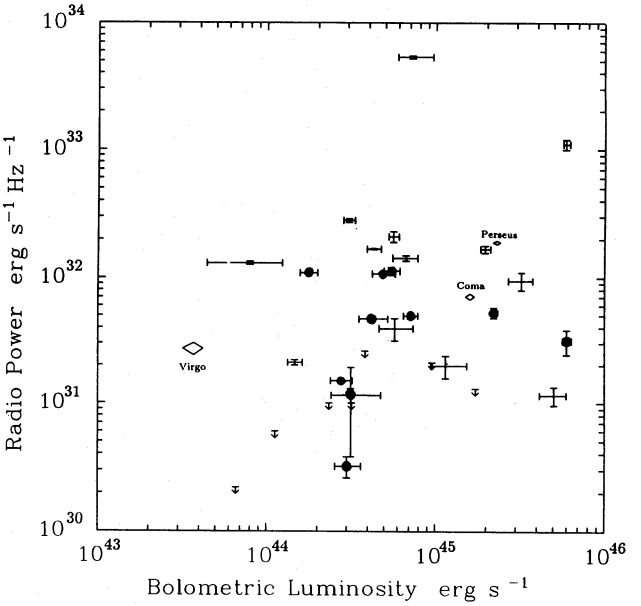

Figure 15. Monochromatic radio luminosity at 1.4 GHz for the brightest cluster radio source against bolometric X-ray luminosity. Sources which are known to be radio tails or are offset from the cluster centre are marked as solid circles.

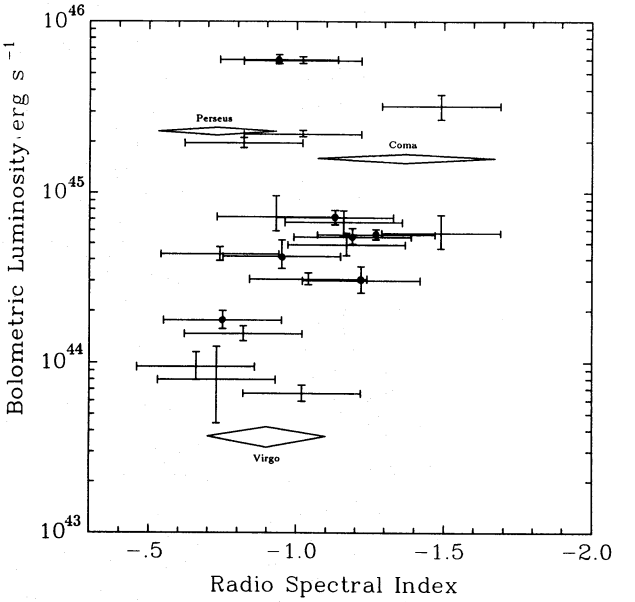

Figure 16. Bolometric luminosity against radio spectral index. Sources which are known to be radio tails or are offset from the cluster centre are marked as solid circles.

luminosities obtained from flux-limited samples with most sources close to the flux limits.

If the *IRAS* fluxes are due to emission from the cluster, they imply that there is a substantial amount of dust around these cD galaxies or there is a population of bright *IRAS* sources in cluster cores where galaxy–galaxy mergers will be most frequent. The first of these possibilities results in enhanced cooling in the cores of these clusters above that expected from the X-ray emission alone. This implies that the mass deposition rates in the cooling flow will be higher as well (Bregman *et al.* 1990). Given the *IRAS* resolution of ~ 1 arcmin it is unlikely that many of the detections are due to other galaxies in the cluster, as they would have to be concentrated very close to the core. Therefore a dust component in the ICM around the cD is the most likely explanation.

The possibility of a large dust content in ICM, which could have been detected by *IRAS* at 100 μm, has been noted by Hu *et al.* (1985) and Dwek, Rephaeli & Mather (1990). If the dust results from recent stripping of dust-rich spirals then the dust should be seen where stripping is most active, i.e. the point at which the ICM pressure begins to exceed the pressure in the ISM of the spiral galaxy (we assume that the first pass of a spiral through gas of this pressure strips the bulk of the available ISM). Even for low-luminosity clusters this region may be hundreds of kiloparsecs from the centre so the dust may appear as a halo. The preference for dust in the outer regions of a cluster would be reinforced by the shorter lifetime of dust toward the centre (where the gas density is highest) due to spluttering (Draine & Salpeter 1979). No systematic study of diffuse *IRAS* emission in clusters has been published, but the 100-μm image of the Virgo cluster in Leggett *et al.* (1987) shows a 'cirrus' ring concentric with M87.

3.7 Radio emission

Strong radio sources are often found in cluster environments (McHardy 1979; Andernach, Waldhausen & Wielebinski 1980; Fanti *et al.* 1982; O'Dea & Owen 1985). The variety in structure and luminosity of these radio sources is large, ranging from wide- and narrow-angle tailed sources to diffuse radio haloes. Fig. 15 shows the X-ray luminosity plotted against the monochromatic radio power at 1.4 GHz. The large scatter demonstrates the diversity of sources found in clusters. Where radio spectral indices were available these have also been plotted against X-ray luminosity (Fig. 16). In general the most powerful sources and those with the steepest spectral indices are found in the largest, most dense clusters, but not all of these clusters contain powerful sources.

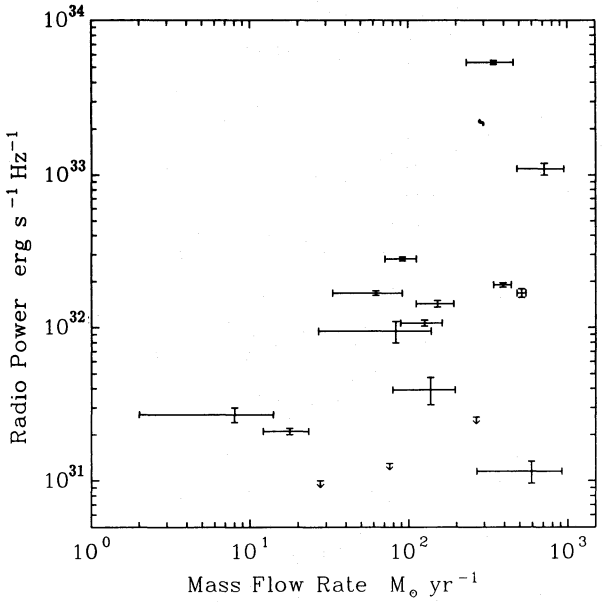

Figure 17. Monochromatic radio luminosity at 1.4 GHz of central radio sources against mass flow rate.

For the radio sources that are related to the central galaxy we plot the radio luminosity against the mass flow rate (Fig. 17). The correlation contains substantial scatter and is only marginally consistent with the result of Burns (1990). (This is primarily due to the inclusion of A478 which has a large cooling flow but a low radio luminosity.) The large scatter between X-ray and radio (and optical and radio) data indicates that the role of the radio source in the energetics of the ICM or member galaxies is small. However, the nature of radio sources is largely determined by their environment. So a trend for brighter radio sources to be found in denser, more X-ray luminous clusters is seen, but with considerable scatter due to the stochastic, short-lived nature of radio galaxies.

4 DISCUSSION

4.1 The 'Beta problem'

A discrepancy between the values for the scaleheight of a cluster estimated from imaging and spectral data ($\beta_{\rm imag}$ and $\beta_{\rm spec}$) has been noted for a number of years (Mushotzky 1984; Jones & Forman 1984). Evrard (1990) has recently performed hydrodynamic simulations which give two systematically different values for $\beta_{\rm spec}$ and $\beta_{\rm imag}$. This is attributed to incomplete thermalization of the gas in the ICM. In order to account for the observational data, Evrard proposes an additional process which preferentially heats the gas in low-temperature clusters, thus lowering $\beta_{\rm spec}$ from 1.2 to 0.7–0.8.

A plot of the measured temperatures and velocity dispersions with the expected relations for $\beta_{\rm spec}=0.5$ and 1.0 (Fig. 2) shows that the majority of the clusters in our sample lie in the region between these two values. The average value of $\beta_{\rm spec}$ is 0.91 with an rms scatter of 0.38 for all 23 clusters or 0.83 with an rms scatter of 0.27 excluding Perseus and A2147, which have values of 1.78 and 1.81. This compares much more favourably with the average value from the imaging data from the *Einstein Observatory* of 0.66 ± 0.10 (Jones & Forman 1984) than the previous value from *HEAO-1* data of 1.2 (Mushotzky 1984). This is due, on the whole, to revisions of the optical velocity dispersions in the past five years following improved measurements with more velocities per cluster and not to changes in measured temperatures or differences in the samples used to calculate $\beta_{\rm spec}$. Fig. 18(a) and (b) show the distribution of $\beta_{\rm spec}$ and $\beta_{\rm imag}$ plotted in histogram form. Both distributions peak at about 0.8, although $\beta_{\rm spec}$ has a 'tail' up to 1.8. For the few clusters for which values of both $\beta_{\rm spec}$ and $\beta_{\rm imag}$ are known there is a general agreement but with several exceptions (Fig. 19), in particular Perseus. A Kolmogorov–Smirnov test on the two sets of β gives a probability of them being drawn from the same parent population of 0.1 per cent, or 0.5 per cent if Perseus and A2147 are excluded, so there are still differences in the samples even if the most discrepant points are ignored.

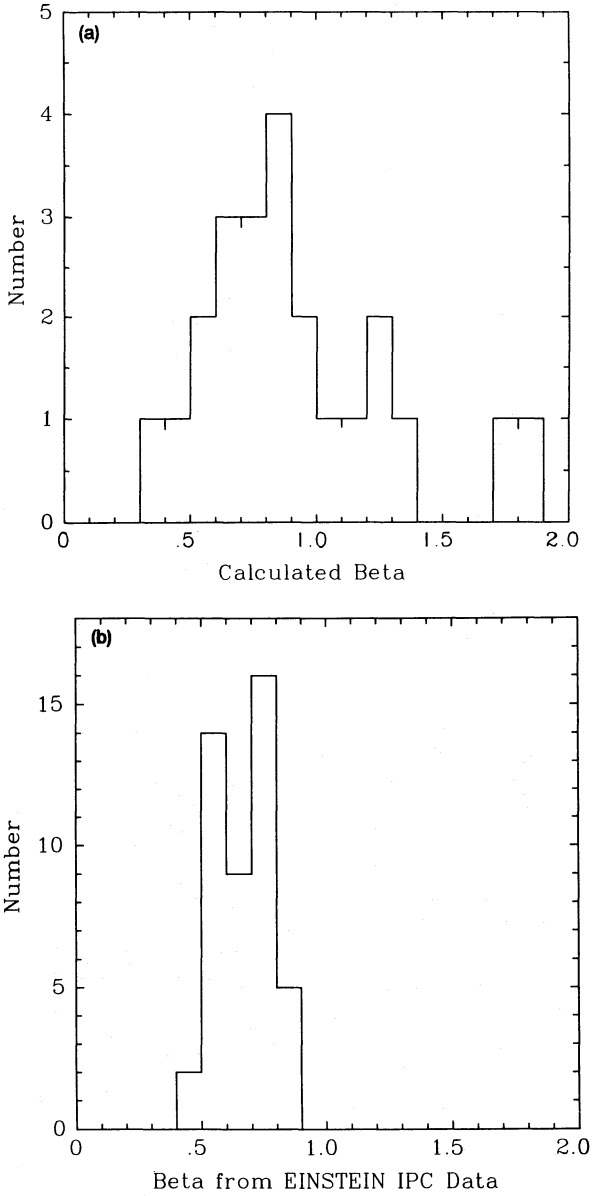

Figure 18. (a) Histogram of calculated beta ($\beta_{\rm spec}$), (b) histogram of imaging beta ($\beta_{\rm imag}$).

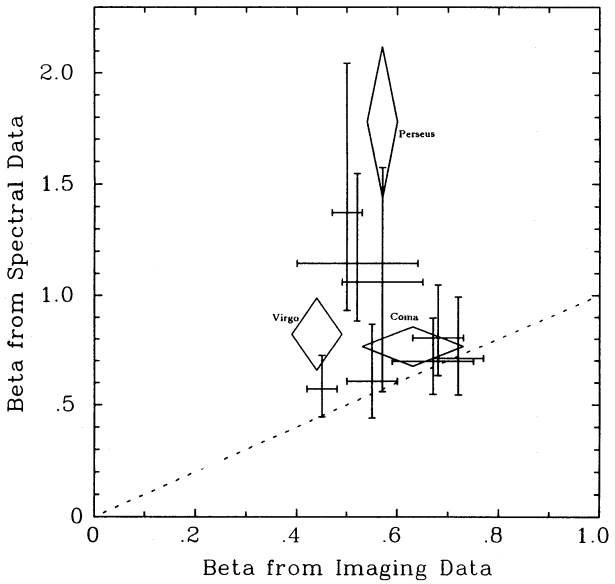

Figure 19. Comparison of values of β_{spec} and β_{imag} where both values have been measured.

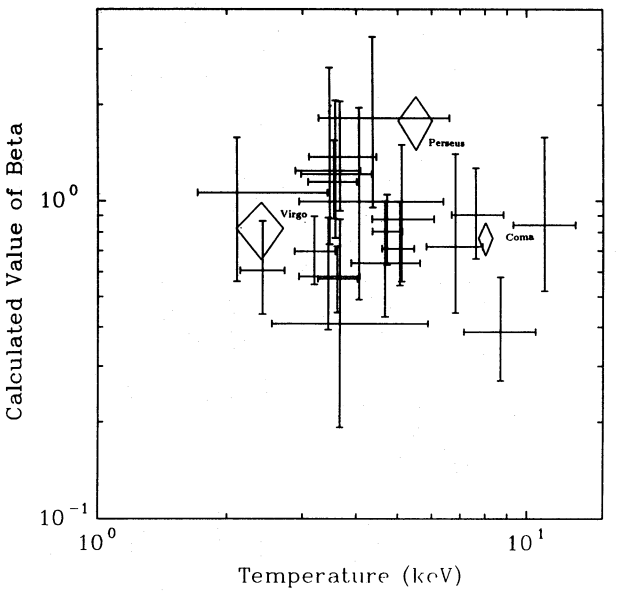

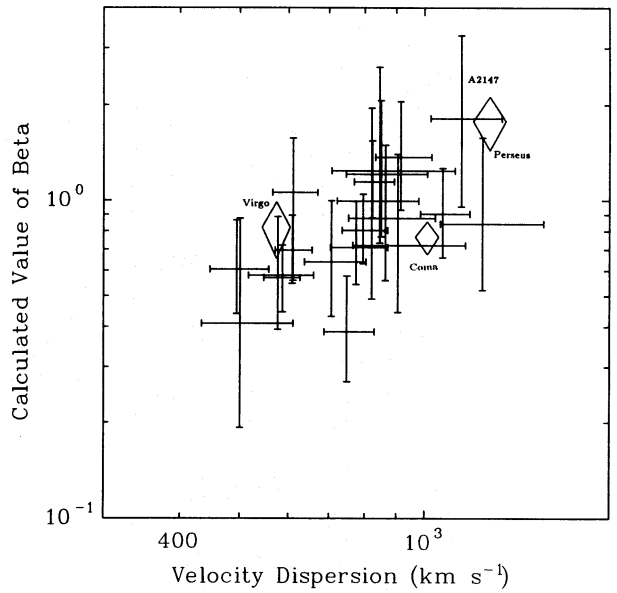

Figure 20. (a) and (b) β_{spec} against temperature and velocity dispersion.

Erroneous values of β_{spec} can result either from over-estimated velocity dispersions or under-estimated temperatures. To differentiate between these two possibilities, β_{spec} is plotted against velocity dispersion and temperature in Figs 20(a) and (b). From these figures, it is clear that the large values of β_{spec} are obtained for clusters with high velocity-dispersions and not low temperatures. This point is strengthened by recent optical work on the Perseus cluster (Fitchett & Smail 1991) where significant velocity substructure is found and other cases where velocity structure is found (e.g. Centaurus, Lucey, Currie & Dickens 1986) and in *N*-body simulations where clusters are found frequently to be contaminated with nearby subclusters in the line of sight (Frenk *et al.* 1990) leading to overestimated velocity dispersions. Perseus demonstrates that even a cluster with a smooth velocity histogram containing over 100 galaxy measurements can be assigned an overestimated value of the velocity dispersion. This common velocity substructure is consistent with the frequent cluster–cluster mergers expected from X-ray cluster evolution (Edge *et al.* 1990). So most of the substructure should be due to bound (sub)clusters (just) pre- or post-merger rather than random line-of-sight alignments. Also, in the case of A2147, Tarenghi *et al.* (1980) note that the velocity dispersion for the early-type galaxies (E and S0) is smaller than that for late-types, as is also the case in Virgo (Binggeli, Tammann & Sandage 1987). There are very few galaxies in the velocity dispersion calculation so it is not possible to exclude the spirals (as is done with Virgo). This dependence on galaxy type is probably related to field galaxies that have recently fallen into the cluster and may affect many other clusters. Therefore we have reason to believe that the two highest values of β_{spec} in this sample have overestimated velocity dispersions. A reduction of 25 per cent in the velocity dispersion (i.e. 1200 to 900 km s^{-1}) would bring the value of β_{spec}, in both cases, down to a value consistent with the rest of the sample.

The clusters with overestimated velocity dispersions lead to a 'flattening' of the temperature–velocity dispersion relation so the simple correlation analysis gives $T \propto \sigma^{1.35}$ rather than the expected $T \propto \sigma^2$. As seen above, there is a trend of β_{spec} with velocity dispersion in Fig. 20(b) ($\beta \propto \sigma^{0.8}$). This trend with velocity dispersion leads to the 'flattening' seen in the temperature–velocity dispersion relation. Even if this trend of β_{spec} with velocity dispersion is not due to overestimation of the velocity dispersions, the basic point that the average is less than one is unchanged. Therefore we conclude that, with the improvement in the optical data, the 'Beta Problem' is resolved and, in the future, cases of $\beta_{spec} > 1$ may be used to identify velocity substructure.

The questions of why $\beta < 1$ (i.e. the gas is 'hotter' than the galaxies) and whether there is any trend with cluster mass (and hence temperature) remain. These relate directly to how the ICM is formed (White 1991). This could either be explained by violent expulsion of gas from galaxies at early

times, heating the ICM (De Young 1978; Thomas & Fabian 1990) or stripping of gaseous haloes from spiral galaxies (Lea & De Young 1976) which occurs preferentially for the galaxies moving fastest through the ICM. The models for violent supernovae-driven winds predict iron and oxygen abundances of about one third and one respectively and an increasing value of β with cluster mass (White 1991) as the escape velocity of poor clusters is close to the wind velocity. As mentioned above, such a trend does appear in the data but probably results from systematically higher velocity-dispersions. Better imaging data and velocity dispersions will provide conclusive evidence for or against galactic wind models thus giving important information on both ICM and galaxy formation and on cluster mass estimates.

4.2 The influence of environment on galactic type

The strongest correlation in the analysis is that between the spiral fraction and the X-ray luminosity, indicating a strong connection between the ICM and the nature of the galaxies moving through it. Ram-pressure stripping is the most obvious mechanism for this. The pressure in the ICM within 1 Mpc of the centre of the cluster is higher than that in the ISM of the Milky Way (10^4 cm^{-3} K) so even a single passage through the cluster must have a significant effect on a spiral galaxy. Radio and optical work on spirals shows weak evidence for stripping (Giovanelli & Haynes 1985) and that spirals transform into S0s. The argument that S0s are stripped spirals is, however, disputed (Dressler 1980b; van den Bergh 1990). The increase in the fraction of ellipticals with galaxy density could be attributed to more mergers (Toomre & Toomre 1972) or more violent agitation of the galaxian potentials by tidal forces (Miller 1988). Alternatively the structural differences between field and cluster galaxies may be due to differences in the local mass density at the time of formation (Evrard, Silk & Szalay 1990).

To this rather contradictory debate, we wish to make an additional observation. The discovery of rapid, on-going evolution of clusters of galaxies (Edge *et al.* 1990; Gioia *et al.* 1990) argues that hierarchical merging is the dominant mechanism in the development of massive clusters. Small clusters, such as Virgo, merge to form larger clusters, such as Coma. The strength of the anticorrelation of spiral fraction and X-ray luminosity implies that, when clusters merge, the fraction of spirals decreases, i.e. galaxies that were spirals must rapidly transform into another form through gas stripping, tidal interaction or mergers with other cluster galaxies. This argues against models in which galaxy type is determined uniquely at the time of formation, as galaxies change their structure with time. Galaxies will enter clusters as spirals, are then stripped to become S0s and later merge with other galaxies to form ellipticals (Toomre & Toomre 1972). This is by no means the only way of explaining the available data but is the most straightforward. The same argument can be made about central cluster galaxies which 'grow' in sympathy with the cluster, suggesting merging as the mechanism for cD evolution (Edge 1991).

To conclude, we note that the formation of galaxies must be affected by the environment in which they are formed, but the subsequent passage through the ICM or interactions with other galaxies may be the deciding factor in their outward appearance. How individual galaxies evolve optically (e.g. the Butcher–Oemler effect) and the magnitude of stripping activity at redshifts beyond 0.3 require further work on combined X-ray and optical samples. For instance, the ability to make galaxy type identifications for clusters at redshifts of 0.5 would allow the X-ray luminosity to spiral fraction correlation to be determined for significantly younger clusters. If rapid stripping does occur then the nearby and distant samples should exhibit the same correlation.

4.3 Cluster masses, mass-to-light ratios and mass components

As no systematic estimates for the total optical luminosity of clusters exist in the literature we have used the Bahcall galaxy number densities to estimate these. For a standard Schechter luminosity function (Colless 1989), the Bahcall number density, N_B, is related to the total optical luminosity, L_B as $L_B = 1.8 \times 10^{10}\, N_B^{1.42}\, h^{-2}\, L_\odot$. By combining the luminosities calculated from the galaxy number densities with estimates of the gravitational mass within 0.5 Mpc from the temperature (assuming hydrostatic equilibrium and a constant β of 0.7), we obtain the values of mass-to-light ratio plotted in Fig. 21. The average M/L (within 0.5 Mpc) is $175 \pm 65\ h\ M_\odot/L_\odot$, which is comparable to previous optical estimates. The absolute value of this ratio depends strongly on the estimation of L_B which is relatively crude. The relative values are not affected by this uncertainty, however, so the small scatter seen in M/L is significant. There is a slight trend for lower M/L at higher temperatures but this is probably related to the selection of the high-temperature clusters as rich, Abell clusters rather than any real increase in L with M.

The estimates for the total optical luminosity can also be used to calculate the ratio of gas mass to galactic mass for an assumed galactic mass-to-light ratio. Taking M_{galaxy}/L_B of 8 (i.e. little or no dark matter in galaxies) as found for S0s and Es (Faber & Gallagher 1979; David *et al.* 1990), gas-to-galactic mass ratios were calculated (Fig. 22). This ratio is scattered between 1 and 2 indicating that the ICM is the dominant luminous baryonic component in the cores of clus-

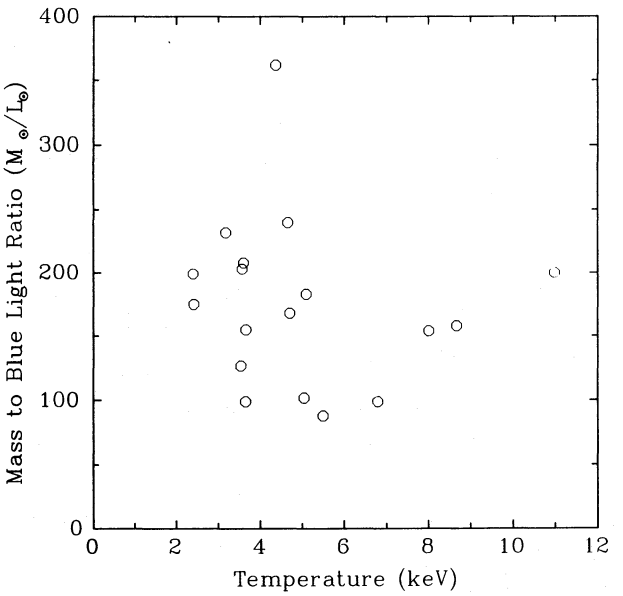

Figure 21. Mass-to-light ratios against temperature.

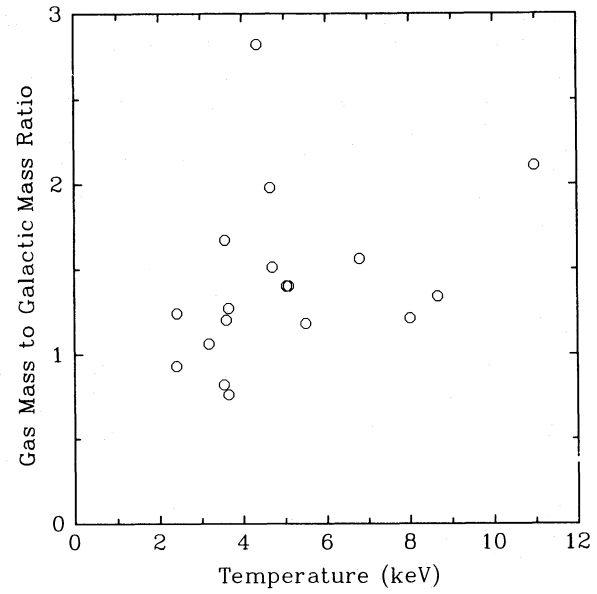

Figure 22. Ratio of gas-to-galactic mass against temperature within 0.5 Mpc.

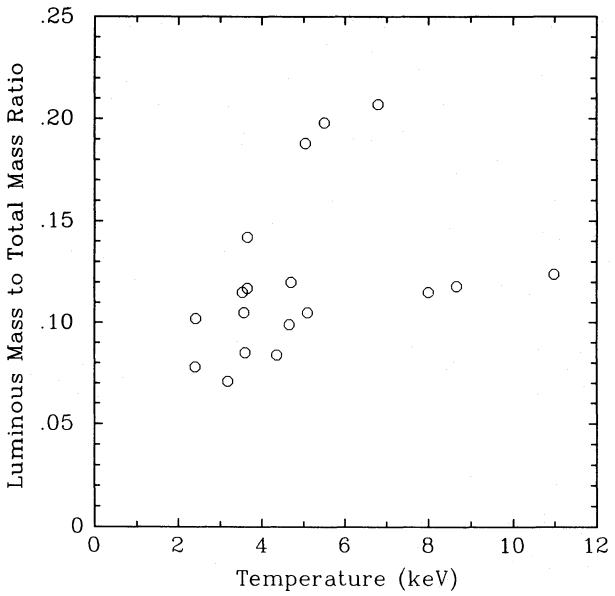

Figure 23. Fraction of luminous, baryonic mass against temperature within 0.5 Mpc.

ters. Due to the more gradual decrease in the gas density compared to the galaxy density (i.e. $\beta < 1$), this gas-to-total mass ratio will increase if larger apertures are taken, therefore these numbers should be seen as lower limits.

David *et al.* (1990) found the value of the gas-to-galactic mass ratio increased from 0.25 to 4 from poor groups to rich clusters, thus agreeing with the result here that the ICM in clusters contains more mass than the galaxies. The strong trend in David *et al.* (1990) is related to the effects of integrating surface brightness profiles to obtain gas masses, their use of five X-ray core radii as an aperture rather than a fixed 0.5 Mpc as used in this work and the presence of a general trend for larger core radii as the cluster temperature increases (Paper I). Many of the clusters above 4 keV have core radii of > 250 kpc so surface brightness profiles must be well determined to beyond 1.2 Mpc, which is not often the case for IPC data. Their result implies a strong increase of gas-to-total mass ratio which is not found in our work (Paper I). This can be understood, since when β is less than one, the ratio of the gas mass to galaxy mass increases with radius and David *et al.* (1990) take systematically larger radii with increasing temperature.

In addition, the total luminous baryonic content can be calculated from the gas and galactic masses within 0.5 Mpc. These baryonic fractions are plotted in Fig. 23 and range between 5 and 20 per cent with a typical value of 10 per cent. This implies that within the cores of clusters 80 to 95 per cent of the mass is non-luminous, which if it applied universally would give $\Omega = 1$. Most of the scatter in the data is due to the variation in the gas mass to total mass discussed in Paper I.

These ratios are dependent largely on the accuracy of the optical luminosities. Therefore any firm conclusions about the exact ratios and the size of the intrinsic scatter can only follow a comprehensive optical study for these clusters, although the results from this work indicate that the ICM is the main contribution to the observed baryonic mass in clusters. If this is correct and all the gas in the ICM has been processed in galaxies, then galaxies have ejected over half their initial mass or disintegrated during the violent ejection.

5 CONCLUSIONS

There are strong relationships between the properties of the intracluster medium, as deduced from observations of their X-ray emission, and the properties of clusters of galaxies from observations of their galactic content. These correlations imply that both the X-ray and optical properties respond to the same potential. Many of the fundamental parameters of the cluster, such as mass, are in fact more easily and more accurately determined from the X-ray data.

(i) There is a significant scatter in the relationship between X-ray luminosity and temperature. This is interpreted as a variation in the ratio of gas mass to total gravitational mass of a factor of three.

(ii) The velocity dispersion is well correlated with temperature and implies values of the β parameter of less than one in agreement with imaging data. This resolves the 'Beta problem'.

(iii) The fraction of spirals in a cluster is closely related to the X-ray luminosity, implying a direct link between galaxy properties and the ICM.

(iv) The absolute magnitude of the central dominant galaxy is related to the X-ray properties of the host cluster. Work using these galaxies as 'standard candles' should take this into account.

(v) The ratio of mass in ICM gas to mass in galaxies is between one and two within the core making the ICM the dominant baryonic component of clusters.

(vi) The total baryonic component of clusters is at least 10 per cent.

All these results can be used to constrain models for the formation and evolution of the ICM and member galaxies.

Future X-ray observations will elucidate many questions about the formation and evolution of clusters and galaxies, as well as putting limits on the nature and distribution of the Dark Matter in clusters.

ACKNOWLEDGMENTS

The authors thank the *EXOSAT* Observatory staff for the smooth operation of the satellite during and after the mission, also to Andy Fabian, Ofer Lahav and especially Richard Mushotzky for comments on the paper and the thesis on which it is based. ACE and GCS acknowledge the support of the SERC through a studentship and Advanced Fellowship. ACE also acknowledges the support of the Royal Society during the completion of this paper.

REFERENCES

Abell, G. O., 1958. *Astrophys. J. Suppl.*, **3,** 211.
Abell, G. O., Corwin, H. G. & Olowin, R. P., 1989. *Astrophys. J. Suppl.*, **70,** 1.
Abramopoulos, F. & Ku, W., 1983. *Astrophys. J.*, **271,** 446.
Andernach, H., Waldthausen, H. & Wielebinski, R., 1980. *Astr. Astrophys. Suppl.*, **41,** 339.
Bahcall, N. A., 1977a. *Astrophys. J. Lett.*, **217,** L77.
Bahcall, N. A., 1977b. *Astrophys. J. Lett.*, **218,** L93.
Bahcall, N. A., 1981. *Astrophys. J.*, **247,** 787.
Beers, T. C., Geller, M. J., Huchra, J. P., Latham, D. W. & Davis, R. J., 1984. *Astrophys. J.*, **283,** 33.
Bhavsar, S. P., 1989. *Astrophys. J.*, **338,** 718.
Binggeli, B., Tammann, G. A. & Sandage, A., 1987. *Astr. J.*, **94,** 251.
Bregman, J. N., McNamara, B. R. & O'Connell, R. W., 1990. *Astrophys. J.*, **351,** 406.
Burns, J. O., 1990. *Astr. J.*, **99,** 14.
Cavaliere, A. & Fusco-Femiano, R., 1976. *Astr. Astrophys.*, **49,** 137.
Colless, M., 1989. *Mon. Not. R. astr. Soc.*, **237,** 799.
Cowie, L. L., Fabian, A. C. & Nulsen, P. E. J., 1980. *Mon. Not. R. astr. Soc.*, **191,** 399.
Cowie, L. L., Hu, E. M., Jenkins, E. B. & York, D. G., 1983. *Astrophys. J.*, **272,** 29.
David, L. P., Arnaud, K. A., Forman, W. & Jones, C., 1990. *Astrophys. J.*, **356,** 32.
De Young, D. S., 1978. *Astrophys. J.*, **223,** 47.
Draine, B. T. & Salpeter, E. E., 1979. *Astrophys. J.*, **231,** 77.
Dressler, A., 1980a. *Astrophys. J. Suppl.*, **42,** 565.
Dressler, A., 1980b. *Astrophys. J.*, **236,** 351.
Dwek, E., Rephaeli, Y. & Mather, J. C., 1990. *Astrophys. J.*, **350,** 104.
Edge, A. C., 1991. *Mon. Not. R. astr. Soc.*, **250,** 103.
Edge, A. C. & Stewart, G. C., 1991. *Mon. Not. R. astr. Soc.*, **252,** 414 (Paper I).
Edge, A. C., Stewart, G. C., Fabian, A. C. & Arnaud, K. A., 1990. *Mon. Not. R. astr. Soc.*, **245,** 559.
Evrard, A. E., 1990. *Astrophys. J.*, **363,** 349.
Evrard, A. E., Silk, J. & Szalay, A. S., 1990. *Astrophys. J.*, **365,** 13.
Faber, S. M. & Gallagher, J. S., 1979. *Ann. Rev. Astr. Astrophys.*, **59,** L5.
Fanti, C. *et al.*, 1982. *Astr. Astrophys.*, **105,** 200.
Fitchett, M. & Smail, I., 1991. Preprint, University of Durham.
Fitchett, M. & Webster, R., 1987. *Astrophys. J.*, **317,** 653.
Frenk, C., White, S. D. M., Efstathiou, G. & Davis, M., 1990. *Astrophys. J.*, **351,** 10.
Gioia, I. M., Henry, J. P., Maccacaro, T., Morris, S. L., Stocke, J. T. & Wolter, A., 1990. *Astrophys. J. Lett.*, **356,** L35.
Giovanelli, R. & Haynes, M. P., 1985. *Astrophys. J.*, **292,** 404.
Green, M. R., Godwin, J. G. & Peach, J. V., 1988. *Mon. Not. R. astr. Soc.*, **234,** 1051.
Gregory, S. A. & Thompson, L. A., 1984. *Astrophys. J.*, **286,** 422.
Hintzen, P. & Scott, J. S., 1979. *Astrophys. J. Lett.*, **232,** L145.
Hintzen, P., Hill, J. M., Lindley, D., Scott, J. S. & Angel, J. R. P., 1982. *Astr. J.*, **87,** 1656.
Hoessel, J. G., Gunn, J. E. & Thuan, T. X., 1980. *Astrophys. J.*, **241,** 486.
Hu, E. M., Cowie, L. L. & Wang, Z., 1985. *Astrophys. J. Suppl.*, **59,** 447.
Johnstone, R. M., Fabian, A. C. & Nulsen, P. E. J., 1987. *Mon. Not. R. astr. Soc.*, **224,** 75.
Jones, C. & Forman, W., 1984. *Astrophys. J.*, **276,** 38.
Jura, M., Kim, D. W., Knapp, G. R. & Guhathakurta, P., 1987. *Astrophys. J. Lett.*, **312,** L11.
Kowalski, M. P., Ulmer, M. P., Cruddace, R. G. & Wood, K. S., 1984. *Astrophys. J. Suppl.*, **56,** 403.
Lea, S. M. & De Young, D. S., 1976. *Astrophys. J.*, **210,** 647.
Leggett, S. K., Clowes, R. G., Kalafi, M., MacGillivray, H. T., Puxley, P. J., Savage, A. & Wolstencroft, R. D., 1987. *Mon. Not. R. astr. Soc.*, **227,** 563.
Loewenstein, M. & Fabian, A. C., 1990. *Mon. Not. R. astr. Soc.*, **242,** 120.
Lucey, J. R., 1983. *Mon. Not. R. astr. Soc.*, **204,** 33.
Lucey, J. R., Currie, M. J. & Dickens, R. J., 1986. *Mon. Not. R. astr. Soc.*, **221,** 453.
McHardy, I. M., 1978. *Mon. Not. R. astr. Soc.*, **184,** 783.
McHardy, I. M., 1979. *Mon. Not. R. astr. Soc.*, **188,** 495.
Materne, J. & Hopp, U., 1983. *Astr. Astrophys.*, **124,** L13.
Melnick, J. & Sargent, W. L. W., 1977. *Astrophys. J.*, **215,** 401.
Miller, R. H., 1988. *Comm. Astrophys.*, **13,** 1.
Mitchell, R. J., Dickens, R. J., Bell Burnell, S. J. & Culhane, J. L., 1979. *Mon. Not. R. astr. Soc.*, **189,** 329.
Mushotzky, R. F., 1984. *Physica Scripta,* Vol. T7, 157.
Mushotzky, R. F., 1988. In: *Hot Thin Plasmas in Astrophysics, NATO ASI*, p. 273, ed. Pallavicini, R., Reidel, Dordrecht.
O'Dea, C. P. & Owen, F. N., 1985. *Astr. J.*, **90,** 927.
Parker, Q. A., MacGillivray, H. T., Hill, P. W. & Dodd, R. J., 1986. *Mon. Not. R. astr. Soc.*, **220,** 901.
Quintana, H. & Melnick, J., 1982. *Astr. J.*, **87,** 972.
Quintana, H., Melnick, J., Infante, L. & Thomas, B., 1985. *Astr. J.*, **90,** 410.
Rhee, G. & Roos, N., 1990. *Mon. Not. R. astr. Soc.*, **243,** 629.
Rothenflug, R. & Arnaud, M., 1985. *Astr. Astrophys.*, **144,** 431.
Schombert, J. M., 1988. *Astrophys. J.*, **328,** 475.
Smith, B. W., Mushotzky, R. F. & Serlemitsos, P. J., 1979. *Astrophys. J.*, **227,** 37.
Struble, M. F. & Rood, H. J., 1987. *Astrophys. J. Suppl.*, **63,** 543.
Tarenghi, M., Chincharini, G., Rood, H. J. & Thompson, L. A., 1980. *Astrophys. J.*, **235,** 724.
Thomas, P. A. & Fabian, A. C., 1990. *Mon. Not. R. astr. Soc.*, **246,** 156.
Toomre, A. & Toomre, J., 1972. *Astrophys. J.*, **178,** 623.
Tremaine, S. D., 1990. In: *Dynamics and Interactions of Galaxies*, p. 394, ed. Wielen, R., Springer-Verlag, Berlin.
Valentijn, E. A. & Bijleveld, W., 1983. *Astr. Astrophys.*, **125,** 223.
van den Bergh, S., 1990. *Astrophys. J.*, **348,** 57.
White, R. E. III, 1991. *Astrophys. J.*, **367,** 69.
Zabludoff, A. I., Huchra, J. P. & Geller, M. J., 1990. *Astrophys. J. Suppl.*, **74,** 1.